

# Quantitative Determination of Magnetization Exchange Rate Constants from a Series of Two-Dimensional Exchange NMR Spectra

Zsolt Zolnai,<sup>†</sup> Nenad Juranić, Dražen Vikić-Topić, and Slobodan Macura\*

Department of Biochemistry and Molecular Biology, Mayo Graduate School, Mayo Clinic and Foundation, Rochester, Minnesota 55905

Received August 22, 1999

A method for quantitative determination of magnetization exchange rate constants (cross-relaxation and chemical exchange) from a series of two-dimensional exchange spectra is presented. The method, the least error matrix analysis (LEMA), combines a series of full matrix calculations at different mixing times in a least-squares manner. LEMA embodies the principal advantages of full-relaxation matrix analysis (FMA) and initial rate buildup (BU) analysis. Like FMA, it takes into account all the relations among the spectral matrix elements and in analogy to BU makes use of their time evolution. By means of calculations, simulations, and experiments, we have shown that LEMA provides the dynamic matrix from a given set of experimental data with errors that are smaller than in either FMA or BU calculations.

## INTRODUCTION

Two-dimensional (2D) exchange spectroscopy encompasses a set of methods designed to monitor incoherent magnetization transfer processes in multisite systems.<sup>1,2</sup> It includes different 2D experiments that provide an efficient way for studying the chemical exchange (EXSY) and cross-relaxation in the laboratory (NOESY) or rotating (ROESY) frame. All these experiments can be described using the same mathematical formalism. Therefore, their quantitative analysis is the same.

The most impressive application of 2D exchange spectroscopy is the use of NOESY for the determination of protein structures in solutions.<sup>3</sup> Although, most often a semiquantitative analysis suffices, it is well recognized that the quantitative interpretation of NOESY data can be even more advantageous.<sup>4–6</sup> Due to smaller spectral distortions, EXSY spectra were already quantitatively interpreted.<sup>7–9</sup>

The biggest obstacles for wider use of quantitative 2D exchange spectroscopy are the many imperfections of macromolecular spectra. Notably, the spectral overlap precludes a proper spectral peak volume integration, the base plane distortions alter the peak volumes, etc. Nevertheless, the new multidimensional multinuclear techniques and the equally important new procedures for uniform or selective deuteration of biological macromolecules may eliminate many practical problems. Then, the principal difficulty left would be the lack of appropriate theoretical analysis.

Here, we present a quantitative analysis of an exchanging system having an arbitrary number of spins at spin sites and arbitrary external relaxation rates. First, we provide the principal relations between the spectral and dynamic matrices, and the relations among the dynamic matrix elements. Then, we recast the formulas for initial buildup rate analysis

(BU) and full-relaxation matrix analysis (FMA) to include a variable number of spins at spin sites. After the error propagation analysis, we describe a novel method for quantitative analysis of 2D exchange spectra, the least error matrix analysis (LEMA).<sup>10</sup> Finally, we demonstrate its use and advantages over BU and FMA on a 10-spin model system, cyclo(L-Pro-Gly). A method closely related to LEMA, also based on our previous error propagation analysis,<sup>11</sup> has been described recently.<sup>12</sup> The main advantage of LEMA is that it does not require any prior knowledge about the system, because it recovers the necessary information from experimental data in an iterative manner.

## BASIC RELATIONS IN THE EXCHANGE SYSTEM WITH UNEQUAL POPULATIONS AND UNEQUAL LEAKAGE RELAXATION RATES

Neglecting other interactions, the incoherent transfer of magnetization (chemical exchange and cross-relaxation) observed in exchange spectra is given by the master equation

$$\dot{\mathbf{m}} = \mathbf{L}\mathbf{m} \quad (1)$$

where  $\mathbf{L}$  is the dynamic matrix (whose elements are the magnetization exchange rate constants  $L_{ij}$  and the autorelaxation rate constants  $L_{ii}$ ) and  $\mathbf{m}$  is the vector of the (observable) deviation of actual magnetization  $\mathbf{M}(t)$  from the equilibrium magnetization  $\mathbf{M}^0$ ,  $\mathbf{m} = \mathbf{M}(t) - \mathbf{M}^0$ . It is convenient to represent the 2D exchange spectrum as a matrix of peak volumes  $\mathbf{A}(\tau_m)$ , where  $\tau_m$  denotes the mixing time. The principle of detailed balance (and microreversibility)<sup>13,14</sup> implies that for a fully relaxed system the 2D exchange spectrum, i.e., the corresponding matrix of peak volumes  $\mathbf{A}(\tau_m)$ , is always symmetric. The volume matrix  $\mathbf{A}(\tau_m)$  is related to the dynamic matrix  $\mathbf{L}$  by<sup>1,2,15</sup>

$$\mathbf{A}(\tau_m) = e^{\mathbf{L}\tau_m}\mathbf{A}(0) \quad (2)$$

For  $\tau_m = 0$ , no magnetization exchange takes place, so  $\mathbf{A}(0)$

<sup>†</sup> On leave from the Mathematical Institute, Knez Mihailova 35, 11000 Beograd, Yugoslavia.

\* To whom correspondence should be addressed: E-mail: macura@mayo.edu. Phone: (507) 284-5917. Fax: (507) 284-8433.

is represented by a diagonal matrix whose elements are proportional to the equilibrium populations of the respective spin sites

$$\mathbf{A}(0) = a_0 \mathbf{N} = a_0 \text{diag}(n_1, \dots, n_p) \quad (3)$$

$a_0$  is the unit spectral peak volume (volume of a single spin), and  $\mathbf{N}$  is the diagonal matrix of spin populations whose elements  $n_i$  denote the number of spins at spin site  $i$ . When the spin sites have different populations, i.e.,  $n_i \neq n_j$ , from eqs 2 and 3 it follows that

$$\mathbf{L}\mathbf{N} = (\mathbf{L}\mathbf{N})^T = \mathbf{N}\mathbf{L}^T \quad (4)$$

We say that a matrix  $\mathbf{L}$  with the property given in eq 4 is quasi-symmetric. In a scalar form, eq 4 becomes

$$n_j L_{ij} = n_i L_{ji} \quad (5)$$

Denote by  $\mathbf{L}^0$  the matrix of normalized magnetization exchange rate constants

$$\mathbf{L}^0 = \mathbf{N}^{-1}\mathbf{L} \quad (6)$$

Note that  $\mathbf{L}^0$  is symmetric

$$L_{ij}^0 = L_{ji}^0 = \frac{L_{ij}}{n_i} = \frac{L_{ji}}{n_j} \quad (7)$$

The normalized magnetization exchange rate constant  $L_{ij}^0$  is related to the first-order chemical exchange rate constant  $k_{ij}$  and cross-relaxation rate constant  $R_{ij}$  by

$$L_{ij}^0 = -R_{ij} + k_{ij} \quad (8)$$

The diagonal elements  $L_{ii}$  of the dynamic matrix depend on all the rates by which the particular site loses magnetization:  $L_{ij}$  represents the magnetization exchange with other sites,  $R_{ii}^{\text{auto}}$  the losses due to autorelaxation (if the site has more than one spin), and  $R_{ii}^{\text{ex}}$  the losses due to external sources of relaxation (all the nonobservable spins, including the paramagnetic centers). Thus

$$L_{ii}^0 = -R_{ii}^{\text{ex}} - (n_i - 1)R_{ii}^{\text{auto}} - \sum_{j \neq i} c_{ji} L_{ji}^0 \quad (9)$$

where

$$c_{ji} = \begin{cases} 1, & L_{ji} > 0 \\ -1, & L_{ji} < 0 \end{cases}$$

For infinitely long mixing times, the system spontaneously returns to the equilibrium, so all the  $L_{ii}^0$  values must be negative. This is emphasized by negative signs in eq 9. The constants  $c_{ij}$  takes into account that the positive cross-relaxation rates (negative NOEs) are associated with dissipative autorelaxation processes<sup>15</sup> and ensures that the inequality

$$L_{ii}^0 + \sum_j |L_{ji}^0| \leq 0$$

holds even in the absence of external relaxation. Therefore, the negative definiteness of a dynamic matrix is preserved for all mixing times, ensuring that the deviation from

equilibrium decreases toward zero over time. For NOESY in the spin diffusion regime and for EXSY,  $L_{ij}^0 > 0$  and  $c_{ij} = 1$ ; for NOESY in extreme narrowing and for ROESY,  $L_{ij}^0 < 0$ , and  $c_{ij} < -1$ .

### INITIAL BUILDUP RATE ANALYSIS

It is convenient to expand eq 2 into a Taylor series<sup>15-20</sup>

$$\mathbf{A}(\tau_m) \mathbf{A}(0)^{-1} = e^{\mathbf{L}\tau_m} = 1 + \mathbf{N}\mathbf{L}^0\tau_m + \frac{1}{2}(\mathbf{N}\mathbf{L}^0)^2\tau_m^2 + \frac{1}{6}(\mathbf{N}\mathbf{L}^0)^3\tau_m^3 + \dots \quad (10)$$

The coefficient at the linear term represents the contribution of a single-step magnetization transfer, at the quadratic the two-step transfer, etc. For sufficiently short mixing times, eq 10 can be truncated after the linear term. Then, the experimentally obtained spectrum  $\mathbf{A}(\tau_m)$  directly maps the normalized magnetization exchange rate matrix

$$\mathbf{L}^0 = (1/\tau_m)\mathbf{N}^{-1}(-1 + \mathbf{A}(\tau_m) \mathbf{A}(0)^{-1}) \quad (11)$$

In a scalar form, eq 11 for normalized cross-peaks becomes

$$\frac{A_{ij}(\tau_m)}{n_i A_{jj}(0)} = \frac{A_{ij}(\tau_m)}{n_j A_{ii}(0)} \approx L_{ij}^0 \tau_m \quad (12)$$

or, using eq 3

$$\frac{A_{ij}(\tau_m)}{n_i n_j a_0} \approx L_{ij}^0 \tau_m \quad (13)$$

Note that in eq 12 each diagonal peak is multiplied by the number of spins at the partner site. Only then, the normalization is independent of the choice of the diagonal.

In practice, owing to the low sensitivity, longer mixing times are used. Then the higher-order terms of the Taylor expansion must be taken into account, and eq 12 becomes

$$\begin{aligned} \frac{A_{ij}(\tau_m)}{n_i A_{jj}(0)} &= \frac{A_{ij}(\tau_m)}{n_j A_{ii}(0)} = L_{ij}^0 \tau_m + \frac{1}{2} \sum_k n_k L_{ik}^0 L_{kj}^0 \tau_m^2 + \dots \\ &= L_{ij}^0 \tau_m + \frac{1}{2} \left\{ \sum_{k \neq i,j} [n_k L_{ik}^0 L_{kj}^0 - L_{ij}^0 (n_i c_{ki} L_{ki}^0 + n_j c_{kj} L_{kj}^0)] + \right. \\ &\quad \left. L_{ij}^0 [n_i (R_{ii}^{\text{ex}} + (n_i - 1)R_{ii}^{\text{auto}} - c_{ji} L_{ji}^0) + n_j (R_{jj}^{\text{ex}} + \right. \\ &\quad \left. (n_j - 1)R_{jj}^{\text{auto}} - c_{ij} L_{ij}^0)] \right\} \tau_m^2 + \dots \quad (14) \end{aligned}$$

The quadratic and higher order terms in eq 13 that correspond to two and higher step transfer are a source of error in the analysis of the linear term. The nonlinear terms can overwhelm the desired linear term because of the magnitude of individual  $L_{ik}$  and  $L_{kj}$  terms, the large number of exchange pathways  $k$ , or the long mixing times (large  $\tau_m$ ). Also, the external relaxation and autorelaxation rates  $R^{\text{ex}}$  and  $R^{\text{auto}}$  contribute to the quadratic and higher order terms.

A practical improvement in buildup analysis can be achieved by normalizing the cross-peaks with their respective

diagonals at the current mixing time (instead at zero mixing time):<sup>21</sup>

$$\begin{aligned} \frac{A_{ij}(\tau_m)}{n_i A_{jj}(\tau_m)} &= L_{ij}^0 \tau_m + \left( \frac{1}{2} \sum_k n_k L_{ik}^0 L_{kj}^0 - n_j L_{ij}^0 L_{jj}^0 \right) \tau_m^2 + \dots \\ &= L_{ij}^0 \tau_m + \frac{1}{2} \left\{ \sum_{k \neq i,j} [n_k L_{ik}^0 L_{kj}^0 - L_{ij}^0 (n_i c_{ki} L_{ki}^0 - n_j c_{kj} L_{kj}^0)] + \right. \\ &\quad \left. L_{ij}^0 [n_i (R_{ii}^{\text{ex}} + (n_i - 1) R_{ii}^{\text{auto}} - c_{ji} L_{ij}^0) - n_j (R_{jj}^{\text{ex}} + \right. \\ &\quad \left. (n_j - 1) R_{jj}^{\text{auto}} - c_{ij} L_{ij}^0)] \right\} \tau_m^2 + \dots \quad (15) \end{aligned}$$

For normalization with the other diagonal  $A_{ii}(\tau_m)$  the same expression is obtained, but with indices  $i$  and  $j$  transposed. Since the quadratic and higher order terms of expansion depend on the position of indices  $i$  and  $j$ , they are affected by the diagonal peak selection. The advantage of normalization in eq 15 over eq 14 is that it reduces the influence of external relaxation in the second-order term. (Note the change of sign in  $R_{jj}^{\text{ex}}$  and  $R_{jj}^{\text{auto}}$  terms in eq 15 versus eq 14.) The arithmetic average of normalized cross-peaks in eq 15 and eq 15 with respect to  $A_{ii}(\tau_m)$  gives even better results, as it eliminates completely the influence of external relaxation and autorelaxation rates in the second-order term

$$\begin{aligned} \frac{1}{2} A_{ij}(\tau_m) \left( \frac{1}{n_i A_{jj}(\tau_m)} + \frac{1}{n_j A_{ii}(\tau_m)} \right) &= L_{ij}^0 \tau_m + \\ &\quad \frac{1}{2} \left( \sum_{k \neq i,j} n_k L_{ik}^0 L_{kj}^0 \right) \tau_m^2 + \dots \quad (16) \end{aligned}$$

The limitations and criteria for the validity of the Taylor expansion are described elsewhere.<sup>20</sup>

#### FULL MATRIX ANALYSIS

The dynamic matrix  $\mathbf{L}$  can be obtained by full matrix analysis, solving eq 2:<sup>5,22-26</sup>

$$\mathbf{L} = (1/\tau_m) \ln(\mathbf{A}(\tau_m) \mathbf{A}(0)^{-1}) \quad (17)$$

For a system that is at  $\tau_m = 0$  in thermal equilibrium,  $\mathbf{N} = \text{diag}\{n_1, \dots, n_p\}$  is positive definite. Hence, the quasi-symmetric matrix  $\mathbf{L}$  has  $P$  real (negative) eigenvalues, and the left eigenvectors corresponding to two different eigenvalues are  $\mathbf{N}$ -orthogonal (see the Appendix). From eq 17 it follows that the dynamic matrix  $\mathbf{L}$  is a function of two matrices that correspond to exchange spectra obtained from the experiments recorded at mixing times  $\tau_m$  and zero. A convenient way for calculating the elements of a dynamic matrix uses the eigensystem of  $\mathbf{A}(\tau_m) \mathbf{A}(0)^{-1}$ . The matrix  $\mathbf{A}(\tau_m) \mathbf{A}(0)^{-1}$  that corresponds to a normalized exchange spectrum can be written as

$$\mathbf{A}(\tau_m) \mathbf{A}(0)^{-1} = \mathbf{U} \mathbf{\Gamma}(\tau_m) \mathbf{V}^T \quad (18)$$

where  $\mathbf{\Gamma}(\tau_m)$  is a diagonal matrix whose elements  $\gamma_i(\tau_m)$  are the eigenvalues of the normalized spectral matrix  $\mathbf{A}(\tau_m) \mathbf{A}(0)^{-1}$ , and the matrices  $\mathbf{U}$  and  $\mathbf{V}$  are the left and right modal matrices. Because  $\mathbf{A}(\tau_m) \mathbf{A}(0)^{-1}$  is quasi-symmetric,  $\mathbf{U} = \mathbf{N} \mathbf{V}$  (see the Appendix). The left and right eigenvectors are equal only when all populations are the same. As a result of the invariance of modal matrices to matrix functions, the

dynamic matrix  $\mathbf{L}$  can be written as

$$\mathbf{L} = \mathbf{U} \mathbf{\Lambda} \mathbf{V}^T = \mathbf{N} \mathbf{V} \mathbf{\Lambda} \mathbf{V}^T \quad (19)$$

where the elements of diagonal matrix  $\mathbf{\Lambda}$  are defined by

$$\Lambda_i = (1/\tau_m) \ln \Gamma_i(\tau_m) \quad (20)$$

From eqs 6 and 19 it follows that

$$\mathbf{L}^0 = \mathbf{V} \mathbf{\Lambda} \mathbf{V}^T \quad (21)$$

or in a scalar form

$$L_{ij}^0 = \sum_k \mathbf{v}_{ik} \mathbf{v}_{kj}^T \lambda_k \quad (22)$$

Thus, full matrix analysis comprises the calculation of eigenvectors and eigenvalues of the dynamic matrix over the eigenvectors and eigenvalues of the normalized spectral matrix  $\mathbf{A}(\tau_m) \mathbf{A}(0)^{-1}$ . The main disadvantage of FMA is that it requires the volume integrals of all spectral peaks, including the diagonals.

#### ERROR PROPAGATION ANALYSIS

When the populations at all spin sites are the same, the exact equation for propagation of errors is described in ref 11. For different populations, the equation becomes

$$\begin{aligned} |\Delta L_{ij}^0| &\approx \left[ \sum_{k,r,s,l} (\mathbf{v}_{ir} \mathbf{v}_{rk}^T n_l \mathbf{v}_{is} \mathbf{v}_{sj}^T)^2 \left( \frac{(1 - \delta_{\lambda_r \lambda_s})(\lambda_r - \lambda_s)^2}{e^{\lambda_r \tau_m} - e^{\lambda_s \tau_m}} \right)^2 + \right. \\ &\quad \left. \left( \frac{\delta_{\lambda_r \lambda_s}}{\tau_m e^{\lambda_r \tau_m}} \right)^2 \right]^{1/2} (\Delta A_{kl}^{\text{norm}})^2 = \epsilon(\tau_m, \mathbf{L}, \Delta \mathbf{A}^{\text{norm}})_{ij} \quad (23) \end{aligned}$$

where  $\lambda$ 's are the eigenvalues and  $\mathbf{v}$ 's are the left eigenvectors of  $\mathbf{L}$ . The error matrix  $\Delta \mathbf{A}^{\text{norm}}$  is normalized to the volume of a single spin at  $\tau_m = 0$ . If the volume errors are equal and uncorrelated (i.e.,  $\Delta A_{kl}^{\text{norm}} = \Delta a = \text{constant}$ ), eq 23 becomes

$$\begin{aligned} |\Delta L_{ij}^0| &\approx \Delta a \left[ \sum_{r,s} (\mathbf{v}_{ir} \mathbf{v}_{sj}^T)^2 \left( \frac{(1 - \delta_{\lambda_r \lambda_s})(\lambda_r - \lambda_s)^2}{e^{\lambda_r \tau_m} - e^{\lambda_s \tau_m}} \right)^2 + \right. \\ &\quad \left. \left( \frac{\delta_{\lambda_r \lambda_s}}{\tau_m e^{\lambda_r \tau_m}} \right)^2 \right]^{1/2} = \epsilon(\tau_m, \mathbf{L}, \Delta a)_{ij} \quad (24) \end{aligned}$$

Equation 24 expresses the error of a dynamic matrix element  $L_{ij}^0$  obtained by full matrix analysis when the error of peak volumes is  $\Delta a^{11}$  ( $\Delta a$  is also normalized to the volume of a single spin at  $\tau_m = 0$ ), Figure 1. Note that eqs 23 and 24 are accurate only for small errors. For both equal and nonequal volume errors,  $|\Delta L_{ij}^0| = |\Delta L_{ji}^0|$  and  $|\Delta L_{ij}| = n_i |\Delta L_{ij}^0|$ .

The errors of individual elements  $|\Delta L_{ij}^0|$  have minima at particular  $\tau_m$  values, Figure 1. The spread of the positions of the minima depends on the topology of the system, and is not known in advance. Thus, even for full matrix analysis, a few experiments at different mixing times are needed. Then,

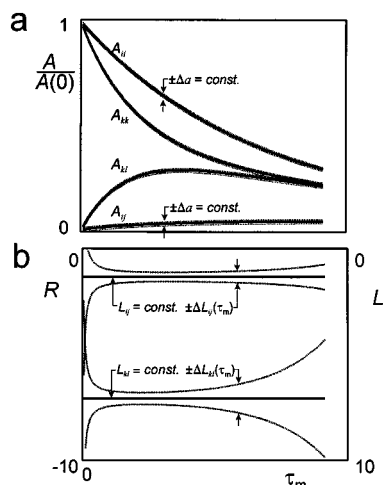


**Figure 1.** Mixing time evolution of spectral peak volumes and their errors in full matrix analysis: (a) According to eq 2, the diagonal peak volumes  $A_{ii}$  and  $A_{kk}$ , monotonously decay from initial values toward zero, whereas the cross-peak volumes  $A_{ij}$  and  $A_{kl}$ , build up from zero and then decay together with diagonals toward zero. When the background noise is the principal source of errors, the peak volumes at all mixing times will have the same error,  $\pm\Delta a$ . (b) The magnetization exchange rate constants  $L_{ij}, \dots, L_{kl}$  are obtained from peak volumes by eq 17, and their error limits from eq 23 or 24. Even when peak volume errors are constant, the magnetization exchange rate constants  $\Delta L_{ij}(\tau_m), \dots, \Delta L_{kl}(\tau_m)$  depend on the mixing time. At extreme mixing times when the cross-peak volumes become vanishingly small, the errors sharply increase. In between, the magnetization exchange rate constant has a minimal error at a characteristic mixing time, different for each spin pair.

instead of analyzing data at only one mixing time, it is much better to analyze all the data available at different mixing times.

### LEAST SQUARES

The method of least squares is a well-known technique for fitting  $N$  data points  $(\tau_k, A_k)$  to a model that has  $M$  adjustable parameters  $L_i$ .<sup>27</sup> It is easily applicable to a fitting function that is linear in its parameters. Let

$$A(\tau) = \sum_{i=1}^M L_i f_i(\tau) \quad (25)$$

be the model function. The method of weighted least squares requires the minimization of

$$E^2 = \sum_{k=1}^N (1/\sigma_k^2) (A_k - \sum_{i=1}^M L_i f_i(\tau_k))^2 \quad (26)$$

with respect to parameters  $L_i$ . The quantities  $\sigma_k^{-2}$  in eq 26 act as weighting factors. The global minimum can be obtained by solving a set of coupled linear equations ( $M$  equations for  $M$  parameters).

If the data points  $A_k$  are samples from a Gaussian distribution with mean  $A(\tau_k)$  and standard deviation  $\sigma_k$ , the maximum-likelihood estimates<sup>27</sup> of parameters  $L_i$ , which maximize the probability that the given set of  $N$  values of  $A_k$  could have occurred, can be obtained by minimizing  $E^2$  from eq 26. For a non-Gaussian distribution one obtains the least-variance estimates<sup>28</sup> of parameters.

The least-squares method does not yield a straightforward solution for nonlinear models, because in this case the partial

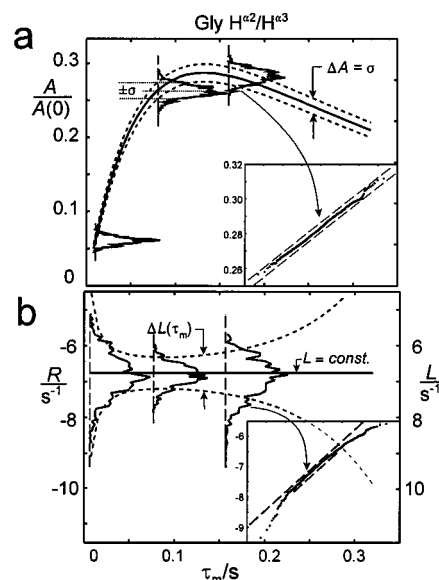


**Figure 2.** Influence of function transformation on distribution of errors: (a) The buildup curve for the Pro  $H^{\alpha 2}/H^{\beta 3}$  spin pair in cyclo-(L-Pro-Gly) is shown with one standard deviation error bound according to the empirical error profile,  $\Delta A = 0.024A + 0.005A(0)$ . The Gaussian distribution curves are determined by 1000 Monte Carlo simulations at each mixing time. The inset shows the probability plot of volume distribution.<sup>34</sup> (b) Upon transformation according to eq 17 the distributions of volume are transformed into distributions of magnetization exchange rate constants. This transformation, however, besides changing the error limits changes the error distributions as well. This is not apparent from the distributions themselves but is clearly visible from the probability plot shown in the inset. The deviation from linearity of the probability plot indicates a deviation from the normal distribution.<sup>34</sup>

derivatives of  $E^2$  are not necessarily linear in the parameters. In this case, an estimate for the parameters can be obtained either by solving a system of coupled nonlinear equations or, directly, by minimizing eq 26. Neither of these two tasks is an easy one, as in both cases the convergence toward a solution strongly depends on the choice of starting value and numerical method used.

**Sample Size and Function Transformation.** To simplify the fitting function, sometimes it is possible to transform the nonlinear model into a linear one. However, after the transformation the errors are usually not normally distributed; therefore, the calculated parameters are not the maximum-likelihood estimates, Figure 2. When the number of data points is small, typically less than 50, the bias introduced by linearization is not significant.<sup>27</sup> To account for the transformation of the dependent variable, the uncertainties must be propagated to the transformed variable. In general, there is no exact solution to this problem; it can only be solved to a first approximation. Thus, the uncertainties in  $f(A)$  are approximately given by

$$\Delta f(A) \approx \sigma_k (df(A)/dA)|_{A_k} \quad (27)$$

Equation 27 is the well-known error propagation formula (used here to derive eqs 23 and 24), and it is a good approximation only for small errors.<sup>29</sup>

**Least-Squares and Buildup Rate Analysis.** The extraction of magnetization exchange rate constants  $L$  from the experimental data  $A_k = A(\tau_k)$  depends on the method for quantification of exchange spectra. Buildup rate analysis

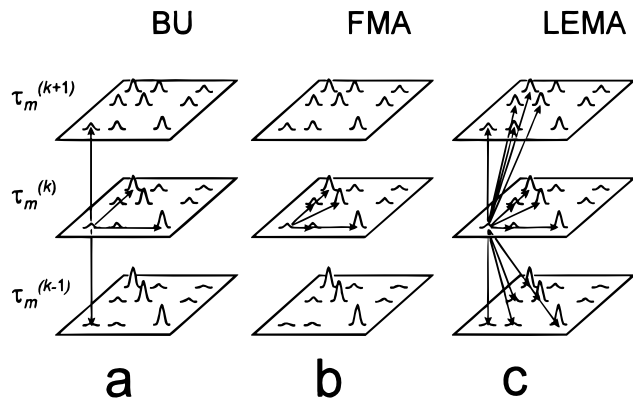


**Figure 3.** Comparison of different methods for quantification of magnetization exchange rate spectra: (a) The buildup rate analysis takes into account the time evolution of the selected volume integral but ignores all others; it needs the diagonal volume for normalization. (b) Full matrix analysis reckons the interdependence of volumes within a spectrum at a given mixing time but ignores the volumes at any other mixing time. (c) Least error matrix analysis considers all the relationships among peak volumes within and between the spectra at all available mixing times in a least-squares manner. Because it uses all available information from a given series of experiments, it is more accurate than full matrix or buildup analysis.

provides the elements of  $\mathbf{L}$  from time evolution of individual cross-peaks. Their values can be obtained by least-squares fitting of the truncated matrix expansion, eq 10. This is equivalent to element-by-element fitting of eq 13 in linear approximation or eqs 14–16 in quadratic approximation. For example, in the quadratic case, when the uncertainties in normalized cross-peak volumes at mixing times are the same, eq 26 becomes

$$E^2 = \sum_{k=1}^N (A_{ij}^{\text{norm}}(\tau_k) - L_{ij}^0 \tau_k - B \tau_k^2)^2 \quad (28)$$

where  $A_{ij}^{\text{norm}}(\tau_k)$  denotes the normalized cross-peak (the left-hand side of eqs 14–16) at the mixing time  $\tau_k$ . The minimum of eq 28 can be found as the solution of a linear coupled system. The uncertainty of the parameter  $L_{ij}^0$  can be obtained by standard methods.<sup>27</sup> The dependence among the cross-peaks within individual 2D spectra in this approach is ignored.

**Least-Squares and Full Matrix Analysis: Least Error Matrix Analysis.** Theoretically, FMA needs only one spectrum for determination of exchange rate constants (eq 17). However, in the presence of noise, the determined exchange rate constants can be very erroneous, especially when the spectrum was obtained at a long mixing time, Figure 1. From the error propagation analysis it follows that for FMA the optimal spectra can be obtained from a limited range of mixing times.<sup>11,30,31</sup> While the FMA simultaneously uses all the peaks at a given mixing time, it ignores the mixing time evolution of cross-peak volumes; i.e., the FMA at a particular mixing time is performed independently from the FMA at other mixing times, Figure 3. Better values of exchange rate constants  $\mathbf{L}$  can be obtained by fitting a series of experimental spectra recorded at different mixing times to eq 2 by nonlinear least squares. Due to the small sample size, instead of fitting eq 2 directly, one can fit its transformed form, the constant function in eq 17. The uncertainties from

$\mathbf{A}^{\text{norm}} = \mathbf{A}(\tau_m) \mathbf{A}(0)^{-1}$  propagate into  $\mathbf{L}$  according to eq 27. For example, if the uncertainties in  $\mathbf{A}^{\text{norm}}$  are unequal and uncorrelated, they propagate as described by eq 23. When the uncertainties are equal (and uncorrelated), the computationally less demanding eq 24 can be used. The cross-relaxation rates  $L_{ij}$  are calculated as the minimum of

$$E^2 = \sum_{k=1}^N \left( \frac{(\mathbf{L}_k)_{ij} - L_{ij}}{\epsilon(\tau_k, \mathbf{L}, \Delta \mathbf{A}^{\text{norm}})_{ij}} \right)^2 \quad (29)$$

The dynamic matrix  $\mathbf{L}_k$  is obtained from the  $k$ th spectrum by FMA. As the weights depend on  $\mathbf{L}$ , the minimization problem (eq 29) is a nonlinear one. If an initial model is available, the weights can be calculated from it, and then the minimization problem (eq 29) becomes a linear least-squares problem. Then

$$L_{ij} = \left[ \frac{\sum_k (\mathbf{L}_k)_{ij}}{\sum_k (\epsilon_k)_{ij}^2} \right] \left/ \left[ \frac{\sum_k 1}{\sum_k (\epsilon_k)_{ij}^2} \right] \right. \quad (30)$$

and

$$\Delta L_{ij} = 1 / \left[ \sum_k \frac{1}{(\epsilon_k)_{ij}^2} \right]^{1/2} \quad (31)$$

where  $\mathbf{L}_k$  is obtained by FMA from the  $k$ th spectrum, and  $\epsilon_k$  is the corresponding weight determined from the particular model. Without a model, the minimum of eq 29 can be found by iteration. The iterative process is enforced by the dependence of weights on the dynamic matrix, eqs 23 and 24. To calculate the weights for the first iteration, a subset of dynamic matrices obtained by FMA at nonextreme mixing times is used. Then, a model dynamic matrix  $\mathbf{L}$  is determined by least squares, and it is used to calculate the weights for the next iteration.

The procedure to determine the best values of magnetization exchange rate constants  $L_{ij}$  from a set of matrices of peak volumes  $\mathbf{A}(\tau_m)$  by the iterative least-squares method is as follows: (i) the  $(q + 1)$ th approximation of dynamic matrix  $\mathbf{L}$  is calculated as

$$L_{ij}^{(q+1)} = \left[ \frac{\sum_k (\mathbf{L}_k)_{ij}}{\sum_k (\epsilon_k^{(q)})_{ij}^2} \right] \left/ \left[ \frac{\sum_k 1}{\sum_k (\epsilon_k^{(q)})_{ij}^2} \right] \right. \quad (32)$$

Again,  $\mathbf{L}_k$  is obtained by FMA from the  $k$ th spectrum (eq 17), and  $\epsilon_k^{(q)}$  is the error propagator defined as

$$\epsilon_k^{(q)} = \begin{cases} \epsilon(\tau_m, \mathbf{L}_k, \Delta \mathbf{A}^{\text{norm}}), & q = 0 \\ \epsilon(\tau_m, \mathbf{L}^{(q)}, \Delta \mathbf{A}^{\text{norm}}), & q > 0 \end{cases} \quad (33)$$

where  $\Delta \mathbf{A}^{\text{norm}}$  is the normalized peak volume error, and  $\mathbf{L}^{(q)}$  is the  $q$ th approximation of the dynamic matrix. The uncertainties of magnetization exchange rates are given by

$$\Delta L_{ij}^{(q+1)} = 1 / \left[ \sum_k \frac{1}{(\epsilon_k^{(q)})_{ij}^2} \right]^{1/2} \quad (34)$$

(ii) For the first iteration ( $q = 0$ ) the sum (in both eqs 32

and 34) is taken over those indices  $k$  that correspond to nonextreme mixing times. In the following iterations all the available mixing times are used.

In the absence of crude errors,  $\mathbf{L}^{(q)}$  converges toward a final  $\mathbf{L}$  after few (usually two) iterations. The final  $\mathbf{L}$  is the best ensemble average for a given set of 2D experiments.

The matrix logarithm (eq 17) (performed once for each spectral matrix) provides information about the peak volume interdependence at a given mixing time, while the weights  $(\epsilon_k^{(q)})_{ij}^2$  enforce the relationship among the cross-peaks at different mixing times. We call this procedure the least error matrix analysis. It is a generalization of BU and FMA, and it effectively combines the advantages of both, Figure 3.

**Implementation.** The LEMA algorithm is implemented in Matlab 4.2 (Mathworks, Inc.). The input into the LEMA program is a vector that contains the mixing times, a vector of matrices that contains the normalized volumes at a given mixing time, a vector of matrices that contains the error for normalized volumes, and a diagonal matrix of populations at spin sites. To obtain the interproton distances, the correlation time, the spectrometer frequency, and the external relaxation have to be provided as well. The matrices and vectors have to be in Matlab format on a file, while the scalars are entered as parameters directly into the program. The output is a matrix that contains the magnetization exchange rate constants, and a matrix with their uncertainties. Inherently, there are no restrictions in the matrix size or the number of matrices. However, the CPU speed and limited memory/disk capacity may restrict the performance of the program. For example, on SGI O<sup>2</sup> for seven  $10 \times 10$  spectral matrices, it takes less than 1 min for two iterations.

### PRACTICAL CONSIDERATIONS

In the absence of experimental errors, any of FMA, BU, or LEMA will provide the exact dynamic matrix from a set of 2D exchange spectra. The differences among the methods become visible while applying them to experimental spectra with finite errors.

**Mixing Time Range.** The most obvious restriction is that the mixing times must be confined to a certain range, which was not known beforehand. The limits are determined by the fastest process that takes place in the system. The shortest mixing time must be long enough to allow at least cross-peaks associated with the fastest process to emerge from the background noise. The fastest process puts an upper limit on mixing time as well, because the difference between the cross-peak and diagonal peak volumes must be larger than the integration error for all allowed mixing times. If these volumes are equal within the existing errors, the equilibrium has been reached, and the information about the rate by which it was established is lost. The existence of the mixing time limit manifests itself as a sharp increase of error limits at extreme mixing times, Figure 1. From eq 24 we obtain

$$\lim_{\tau_m \rightarrow 0} |\Delta L_{ij}^0| \approx \Delta a / \tau_m \rightarrow \infty \quad (35)$$

Thus

$$\tau_m^{\min} \approx \Delta a / \Delta L_{ij}^{\max} \quad (36)$$

Taking (arbitrarily)  $\Delta L_{ij}^{\max} \leq (1/3)|L_{ij}^{\max}|$ , we find

$$\tau_m^{\min} \approx 3\Delta a / |L_{ij}^{\max}| \quad (37)$$

For example, if  $\Delta a = 1\%$  and  $L_{ij}^{\max} = 7 \text{ s}^{-1}$ , we find that  $\tau_m^{\min} \approx 5 \text{ ms}$ .

For the upper limit of the mixing time

$$\lim_{\tau_m \rightarrow \infty} |\Delta L_{ij}^0| \approx \Delta a \frac{\nu_{im}\nu_{jm}e^{+|\lambda^{\max}|\tau_m}}{\tau_m} \rightarrow \infty \quad (38)$$

where  $\nu_{im}\nu_{jm}$  are the eigenvector components associated with the maximal eigenvalue  $\lambda^{\max}$ ;  $\lambda^{\max} < 0$  because  $\mathbf{L}$  is a negative definite matrix. The rate by which the errors increase when  $\tau_m \rightarrow \infty$  depends on the maximum eigenvalue  $|\lambda^{\max}|$ , i.e., on the topology of the system. It is convenient to assume that the fastest process in the system is isolated, so eq 38 can be applied to an isolated spin pair.<sup>31</sup> In NOESY spectra of proteins, this is a good approximation, since the cross-relaxation between the geminal protons ( $r = 1.75 \text{ \AA}$ ) is approximately 4 times faster than the cross-relaxation with the next nearest neighbor ( $r = 2.2 \text{ \AA}$ ). It is easy to see from eqs 23 and 24 that the additional spins necessarily augment the rate of error increase. Thus, the maximal mixing time estimated from the isolated spin pair approximation sets the upper limit for the multispin system as well. The maximum mixing time can be determined from

$$\frac{\Delta L^{\max}}{|L^{\max}|} \approx \Delta a \frac{e^{+2|L^{\max}|\tau_m^{\max}}}{2\tau_m^{\max}} \quad (39)$$

by presetting the maximal allowable  $\Delta L/L$  error. For example, if we allow  $\Delta L/L \leq 1/3$ , the maximal mixing time  $\tau_m^{\max}$  can be estimated from

$$\frac{1}{3\Delta a} \approx \frac{e^{2|L^{\max}|\tau_m^{\max}}}{2\tau_m^{\max}} \quad (40)$$

where  $\Delta a$  is the volume integration error. For  $\Delta a = 1\%$  and  $L^{\max} = 7 \text{ s}^{-1}$  the maximal mixing time is around 170 ms. Thus, for a system with  $L^{\max} = 7 \text{ s}^{-1}$  the optimal mixing time range extends from 5 to 170 ms. Outside these limits the error for the fastest process grows beyond acceptable limits.

**Estimation of Peak Volume Errors.** A good estimate of peak volume errors is a principal prerequisite for error propagation analysis. The standard approach requires repetition of the same experiment many times, and estimation of the volume errors by statistical analysis. Since the data acquisition and processing are time-consuming, this approach is not practical in the case of 2D exchange spectra. Instead, the error estimates are extracted from a set of spectra recorded at different mixing times. Since the experiments are performed under variable conditions, the error estimation procedure has to be modified accordingly.

Exploiting the symmetry of 2D exchange spectra, the average cross-peak volume is determined as the arithmetic

mean of symmetric peak pairs

$$A_{ij}^{\text{norm}} = \frac{(1/2)(A_{ij} + A_{ji})}{(1/n)\sum_k A_{kk}(0)} \quad (41)$$

and an estimate of the cross-peak volume error is obtained from the difference in volumes of the pairs

$$\Delta A_{ij}^{\text{vi}} = \frac{(1/2)|A_{ij} - A_{ji}|}{(1/n)\sum_k A_{kk}(0)} \quad (42)$$

$\Delta A^{\text{vi}}$  reflects the quality of a spectrum at a given mixing time (e.g., signal-to-noise ratio, baseplane distortions, etc.); thus, it is volume-independent.

The volume-dependent error may come from the volume integration routine (e.g., from the variable size and position of the window), long-term instability of the temperature, instrument, etc., and influences mostly the diagonal peaks. For the diagonal volumes a new procedure for error estimation needs to be devised because the diagonals are unique in a 2D spectrum. One possibility is to use the mixing time evolution of total magnetization, expressed as a total integrated volume  $A^\Sigma$

$$A^\Sigma = A^0 e^{-R^* \tau_m} \quad (43)$$

Equation 43 is based on the exact relation<sup>32</sup>

$$\sum_i \dot{m}_i = -\sum_i [R_{ii}^{\text{ex}} + (n_i - 1)R_{ii}^{\text{auto}}] m_i \quad (44)$$

that in diamagnetic systems ( $R_{ii}^{\text{ex}} = \text{constant}$ ) and the spin diffusion limit ( $R_{ii}^{\text{auto}} \approx 0$ ) simplifies to

$$\sum_i \dot{m}_i = -R^* \sum_i m_i \quad (45)$$

In general,  $R^*$  only approximates the sum of autorelaxation and external relaxation rates, but in diamagnetic molecules in the spin diffusion regime it represents the external relaxation rate common for all spins.

The error of total volume at a given mixing time  $\Delta A(\tau_m)$  is calculated as the deviation of total volume from the fitted model volume

$$\Delta A^\Sigma(\tau_m) = \sum_{ij} A_{ij}^{\text{norm}}(\tau_{m_k}) - A^0 e^{-R^* \tau_m} \quad (46)$$

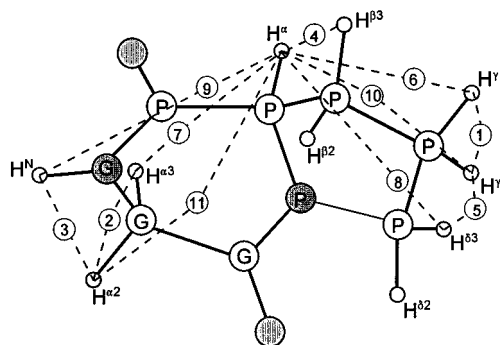
It is then distributed among all peaks assuming constant relative errors. Thus, the volume proportional error  $\Delta A^{\text{vp}}$  becomes

$$\Delta A_{ij}^{\text{vp}} = A_{ij}^{\text{norm}}(\Delta A^\Sigma/A^\Sigma) \quad (47)$$

The overall maximal error is the sum of the constant error  $\Delta A^{\text{vi}}$  and volume proportional error  $\Delta A^{\text{vp}}$

$$\Delta A_{ij} = \Delta A_{ij}^{\text{vi}} + A_{ij}^{\text{norm}}(\Delta A^\Sigma/A^\Sigma) \quad (48)$$

Chart 1



Therefore, the general behavior of maximal volume error may be formulated as

$$\Delta A^{\text{norm}} = \alpha + \beta A^{\text{norm}} \quad (49)$$

where the superscript indicates that the volumes are normalized to the volume of a single spin. To obtain an estimate for the errors of actual experimental data, we used eq 48; for Monte Carlo simulations we fitted the error model eq 49 to the experimental errors.

#### CASE STUDY: CYCLO(L-Pro-Gly)

We illustrate the presented method on a rigid 10-spin system: cyclo(L-Pro-Gly) with known X-ray structure.<sup>33</sup> The protons were attached to the X-ray structure, and their positions were optimized by energy minimization in Quanta (Molecular Simulations, Inc.). At 233 K, the dipeptide is apparently rigid and it most likely tumbles isotropically and has cross-relaxation rates up to  $10 \text{ s}^{-1}$ , like small proteins.

**Experimental Details.** A series of 2D exchange spectra (NOESY) of cyclo(L-Pro-Gly) (Chart 1) in a 3:1 v/v mixture of  $\text{H}_2\text{O}/\text{DMSO}$  has been recorded at 233 K on a Bruker AMX 500 spectrometer, with mixing times of 0.000 06, 0.01, 0.02, 0.03, 0.04, 0.08, 0.16, 0.32, 0.64, and 1.28 s. The spectral data were processed using the Felix 95 (MSI Inc., San Diego, CA) software package. The peak volumes were determined by direct integration. Because of the severe spectral overlap between Pro  $\text{H}^{\beta 2}$  and Pro  $\text{H}^{\gamma 3}$ , their peak volumes were measured together and the respective component volumes were separated by the hybrid matrix approach using the known crystal structure. At  $\tau_m = 80 \text{ ms}$  we also recorded the natural abundance [ $^1\text{H}-^{13}\text{C}$ ] HSQC-NOESY spectrum in which all the peaks were resolved except Pro  $\text{H}^{\beta 2}$  and Pro  $\text{H}^{\gamma 3}$ . The relative peak volumes of the newly resolved peaks agreed with the ratios predicted by the model. Figure 4a shows the cumulative plots of volume errors for all peaks and the best fit according to eq 43. Figure 4b shows the sum of volumes of all peaks at given mixing times, and the best fit according to eq 49. We found that the error can be represented as 2.4% of the current peak volume ( $\beta = 0.024$ ) plus 0.5% of the diagonal (single spin) line at  $\tau_m = 0$  ( $\alpha = 0.005$ ).

**Computer Simulations.** To check and evaluate the three methods for cross-relaxation rate determination, we used the Monte Carlo algorithm. The simulated data sets were generated, adding a noise with experimentally deduced parameters to the theoretical (model) volume values. For simulations we used only the first seven experimental mixing

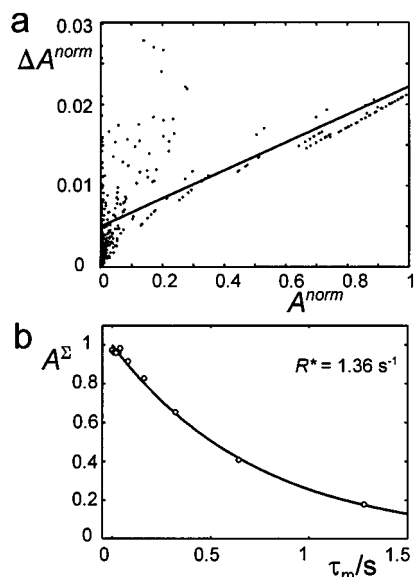


**Figure 4.** Experimental peak volume errors from direct integration of 10 2D spectra of cyclo(L-Pro-Gly): (a) Cumulative plot of all volume errors and the best fit according to eq 40. The errors for cross-peaks are taken from the difference between symmetrical partners. For diagonals, the errors are estimated from the plot in (b). See the text for details. (b) Total magnetization “volume” as a function of mixing time and the least-squares fit according to eq 38b. The deviations of individual points from the smooth curve were used to calculate the volume proportional errors. See the text for details.

times, 0.000 06, 0.01, 0.02, 0.03, 0.04, 0.08, and 0.16 s, because for the longer ones the process of generating feasible volume matrices became extremely inefficient. At each mixing time 1000 data sets (volume matrices) were generated using eq 2, and a white noise was added. The simulated data were processed by LEMA (eqs 31–33), FMA at  $\tau_m = 80$  ms mixing time (eq 17), and BU (by fitting eq 16). As a result, three sets containing 1000 dynamic matrices each were obtained. For the BU fitting of geminal proton pairs only the first five mixing times were used, because at mixing times longer than 40 ms the BU curves exhibit maxima, rendering the quadratic fit unsatisfactory.

**Results.** The mean values and the standard deviations of the model and simulated and calculated cross-relaxation rates

**Table 1.** Comparison of Simulated and Experimental LEMA, BU, and FMA Magnetization Exchange Rates in Cyclo(L-Pro-Gly) for Selected Spin Pairs

spin pair	$L_{\text{model}},^b \text{ s}^{-1}$	$(L \pm \Delta L)^a/\text{s}^{-1}$					
		$\text{LEMA}_{\text{sim}}^c$	$\text{BU}_{\text{sim}}$	$\text{FMA}(\tau_c = 0.08 \text{ s})_{\text{sim}}$	$\text{LEMA}_{\text{exp}}^d$	$\text{BU}_{\text{exp}}$	$\text{FMA}(\tau_c = 0.08 \text{ s})_{\text{exp}}$
1 ProH $\gamma^3$ –ProH $\gamma^2$	7.192 ± 0.30	7.217 ± 0.169	7.302 ± 0.644	7.228 ± 0.355	6.411 ± 0.179	8.257 ± 0.572	5.858 ± 0.329
2 GlyH $\alpha^3$ –GlyH $\alpha^2$	6.760 ± 0.28	6.788 ± 0.174	6.820 ± 0.591	6.781 ± 0.302	7.521 ± 0.272	9.174 ± 0.605	7.451 ± 0.467
3 GlyH $\beta^N$ –GlyH $\alpha^2$	1.325 ± 0.14	1.328 ± 0.069	1.384 ± 0.137	1.329 ± 0.122	1.528 ± 0.106	1.599 ± 0.111	1.523 ± 0.185
4 ProH $\alpha$ –ProH $\beta^3$	1.086 ± 0.13	1.086 ± 0.074	1.126 ± 0.144	1.081 ± 0.124	1.198 ± 0.094	1.208 ± 0.104	1.199 ± 0.168
5 ProH $\gamma^2$ –ProH $\beta^3$	0.475 ± 0.04	0.471 ± 0.105	0.652 ± 0.171	0.470 ± 0.184	0.458 ± 0.150	0.617 ± 0.097	0.456 ± 0.267
6 ProH $\alpha$ –ProH $\gamma^3$	0.446 ± 0.04	0.450 ± 0.077	0.457 ± 0.146	0.448 ± 0.129	0.557 ± 0.084	0.556 ± 0.095	0.542 ± 0.149
7 ProH $\alpha$ –GlyH $\alpha^3$	0.427 ± 0.03	0.426 ± 0.065	0.436 ± 0.131	0.422 ± 0.115	0.191 ± 0.076	0.147 ± 0.090	0.216 ± 0.136
8 ProH $\alpha$ –ProH $\beta^3$	0.121 ± 0.02	0.125 ± 0.071	0.127 ± 0.136	0.123 ± 0.120	0.138 ± 0.079	0.095 ± 0.089	0.138 ± 0.140
9 ProH $\alpha$ –GlyH $\beta^N$	0.082 ± 0.009	0.082 ± 0.046	0.077 ± 0.105	0.081 ± 0.085	0.113 ± 0.052	0.099 ± 0.089	0.108 ± 0.097
10 ProH $\alpha$ –ProH $\gamma^2$	0.065 ± 0.008	0.064 ± 0.075	0.086 ± 0.138	0.071 ± 0.130	0.055 ± 0.084	0.070 ± 0.090	0.040 ± 0.148
11 ProH $\alpha$ –GlyH $\alpha^2$	0.049 ± 0.005	0.048 ± 0.065	0.063 ± 0.129	0.043 ± 0.113	0.090 ± 0.076	0.004 ± 0.088	0.061 ± 0.135

<sup>a</sup> All errors are  $\pm \sigma$  (one standard deviation). <sup>b</sup> Cross-relaxation rates from the X-ray structure optimized by the combined steepest descent and adopted Newton–Raphson method; the error limits were estimated as in ref 10. <sup>c</sup> sim, magnetization exchange rate constants from 1000 Monte Carlo simulated spectral volume matrices at seven experimental values of mixing times. The volume integral error  $\Delta A$  has a Gaussian distribution around the mean volume  $V$ , calculated from the model. The empirically found volume error is used:  $\Delta A^{\text{norm}} = 0.024A^{\text{norm}} + 0.005$ . <sup>d</sup> exp, from experimental spectral volume matrices recorded at 0.000 06, 0.01, 0.02, 0.03, 0.04, 0.08, and 0.16 s mixing times. Individual volume errors are calculated as described in the text.

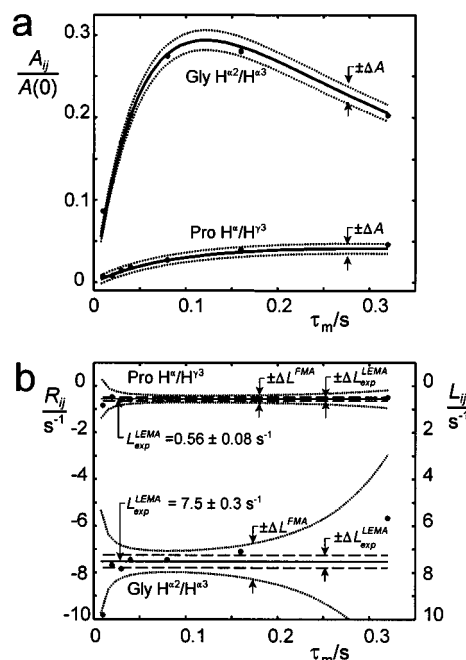


**Figure 5.** Experimental magnetization exchange rate constants and their errors for selected spin pairs from cyclo(L-Pro-Gly).

for selected spin pairs are shown in Table 1. Figure 5 shows the typical buildup curves and experimental volume integrals for two spin pairs. The experimental and simulated data sets were processed almost identically. The only difference is that the actual experimental errors were used instead of the fitted ones.

## DISCUSSION

For the sake of completeness of quantitative analysis we derived the basic equations of 2D exchange spectroscopy in terms of arbitrary spin populations. Such an analysis has not been presented except in some special cases.<sup>9,14,15</sup> As eqs 4–16 indicate, an exact quantitative analysis requires the knowledge of spin populations even if they are typically in a range of 1–3. However, the inclusion of spin populations becomes increasingly important as the fractional deuteration techniques become very popular for larger macromolecules.

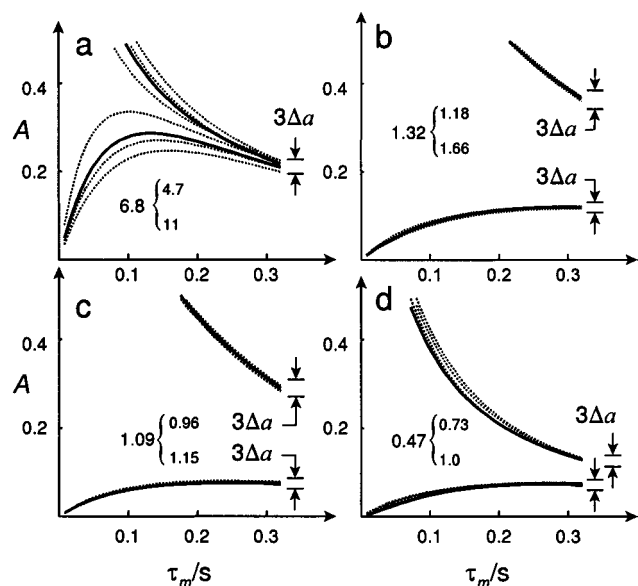


**Figure 6.** Failure of the full matrix analysis at longer mixing time. Shown are the simulated buildup curves (full lines) for cyclo(L-Pro-Gly) calculated from the known structure under the actual experimental conditions ( $\tau_c = 3.8$  ns,  $\omega_o/2\pi = 500$  MHz). The additional (dashed) curves were obtained by Monte Carlo simulation at  $\tau_m = 0.32$  s, allowing spectral peak volumes to vary randomly within the empirically obtained error limits. The arrows at the right of the curves represent the experimental estimate of  $\pm 3\sigma$ . Although all curves at  $\tau_m = 0.32$  s approach the model values within the error limits ( $\pm 2\sigma$ ), the calculated magnetization exchange rates vary greatly: (a) Gly  $H^{\alpha 3}/H^{\alpha 2}$ ; (b) Gly  $H^N/H^{\alpha 2}$ ; (c) Pro  $H^{\alpha}/H^{\beta 3}$ ; (d) Pro  $H^{\gamma 2}/H^{\delta 3}$ . The numbers in the plots represent the model value of cross-relaxation rate constants and the extreme cross-relaxation rates found in the simulations.

There, due to spin dilution, the proton populations can easily vary beyond an order of magnitude. The extension of quantitative analysis to isotope-diluted systems is not straightforward, but it is based on the equations derived here.<sup>35</sup>

It is important to consider the limited applicability of FMA outside a certain range of mixing times because the origin of such a limitation is not obvious. An example when the FMA fails at even moderately long mixing times is illustrated in Figure 6. The buildup curves shown at  $\tau_m = 0.32$  s have the same volumes as the model volumes (full lines) within the limits of the estimated experimental errors (indicated by arrows); however, they correspond to different dynamic matrices of cyclo(L-Pro-Gly). The numbers in the drawing show the model values and the extremes found for each magnetization exchange rate constant. For example, the relative errors of cross-peaks and diagonal peaks of Gly  $H^{\alpha 3}/H^{\alpha 2}$  (Figure 6a) are 5% whereas the relative error of the cross-relaxation rate constant is 62% ( $L^{\text{model}} = 6.8$  s<sup>-1</sup>;  $L^{\text{max}} = 11$  s<sup>-1</sup>). Similarly, for Pro  $H^{\gamma 2}/H^{\delta 3}$ , the input volume error  $\Delta A/A$  is 6% (for diagonal) and 9.5% (for cross-peak volume), but the error in the cross-relaxation rate constant  $\Delta L/L$  is larger than 113% ( $L^{\text{model}} = 0.47$  s<sup>-1</sup> and  $L^{\text{max}} = 1.0$  s<sup>-1</sup>). On the other hand, in spite large errors for some  $L$  values, other  $L$  values may be quite accurate. Such an example is presented in Figure 6c where for Pro  $H^{\alpha}/H^{\beta 3}$   $\Delta A/A$  of 4.2% for diagonals and 9.3% for cross-peaks propagates into  $\Delta L/L$  of 12% ( $L^{\text{model}} = 1.09$  s<sup>-1</sup> and  $L^{\text{min}} = 0.96$  s<sup>-1</sup>). The nonuniform propagation of errors can be explained by eqs 23 and 24. At longer mixing times the errors are dominated by the maximal eigenvalue term  $\exp(+|\lambda^{\text{max}}|\tau_m)/\tau_m$ . Since

the exponential terms are weighted by corresponding eigenvector components, predicting which magnetization exchange rate constant fails first is not easy. However, it is reasonable to expect that the largest  $L$  values have the largest weights for  $\lambda^{\text{max}}$  (eq 22) and, therefore, at longer mixing times the largest errors. The errors of other  $L$  values are difficult to predict since the weights of  $\lambda^{\text{max}}$  are not known beforehand. A general rule is that the largest  $L$  values fail first and that the smaller  $L$  values can still be accurate if they are remote from the fast ones. For the example presented in Figure 6, the principal source of error is the equality of cross-peaks and diagonal peaks within the experimental error for geminal pairs (only Gly  $H^{\alpha 3}/H^{\alpha 2}$  is shown in Figure 6a). The equality of volumes inside the error limits implies that the equilibrium has been reached, and the information about the rate of the approach toward the equilibrium is lost. An erroneous  $L$  for any geminal pair necessarily distorts  $L$  values for other spin pairs. The total effect is that the errors for processes that involve geminal protons become excessively large, perturbing the other proximal processes. However, the remote exchange processes may still have reasonably small errors.

The general dependence of  $\Delta L$  on the mixing time and exchange rate constant itself is illustrated in Figure 1. It shows the buildup curves and  $\Delta L$  values for two spin pairs from cyclo(L-Pro-Gly) (Gly  $H^{\alpha 3}/H^{\alpha 2}$ ,  $L^{\text{model}} = 6.76$  s<sup>-1</sup>; Pro  $H^{\alpha}/H^{\beta 3}$ ,  $L^{\text{model}} = 0.446$  s<sup>-1</sup>). The error of the faster process increases much faster than the error of the slower process. Also, it is important to note that even for volume errors equal and constant through the mixing time range,  $\Delta L$  depends on the mixing time and on  $L$ . This dependence is quantitatively expressed by eq 24. In the general case eq 24 is not obvious, but its properties can easily be understood when reduced to the isolated spin pair.<sup>31</sup>

It is important to note that each  $L_{ij}$  has its own mixing time at which  $\Delta L_{ij}$  is minimal. This implies that instead from a single FMA, better  $L_{ij}$  values can be obtained from a series of FMAs at mixing times where the individual errors are minimal. Such an approach, although it would yield better  $L_{ij}$  values, is inefficient, since all the  $L_{ij}$  values acquired aside from the error minimum would be ignored. It is much better to use all available  $L_{ij}$  values calculated at different mixing times and to average them according to the rules of superposition of errors. This is expressed by eq 30 that averages the  $L$  values calculated at different mixing times. Their errors  $\epsilon_k$  are combined by eq 31. However, since neither the  $L_k$ 's nor their errors are measured directly, it is necessary to consider the conditions under which eqs 30 and 31 are valid.

Equations 30 and 31 yield the maximum likelihood values only if the logarithmic transformation<sup>17</sup> preserves the Gaussian character of the distribution, which needs to be tested independently. We carried that out by testing the distributions generated by 1000 Monte Carlo simulations of FMA at seven mixing times. Figure 2a shows the buildup curve (full line) and the empirical error limits (dashed lines) for Gly  $H^{\alpha 3}/H^{\alpha 2}$ . The three histograms show the distribution of input volumes around the model values in 1000 Monte Carlo simulations. The transformation of model volume matrices, according to eq 17, gives the constant  $L$  for all mixing times (full line, Figure 2b). Similarly, eq 23 transforms the volume errors (dashed lines in Figure 2a) into magnetization exchange rate constant errors (dashed lines in Figure 2b).

The transformation of 1000 Monte Carlo volume matrixes generates 1000 magnetization exchange rate constants around the model value. Their distribution needs to be tested for normality.

All distributions of both the volume and magnetization exchange rate constants were subjected to a normality test using probability plots.<sup>34</sup> The insets in Figure 2 show two probability plots which, if close to straight, confirm the Gaussian character of the distribution. Since the Monte Carlo simulations used Gaussian distribution to generate the volume errors, the volume probability plots are straight, like the one shown in Figure 2a. All the magnetization exchange rate constant distributions except one were also Gaussian. The only exception, shown in Figure 2b, occurs at the longest mixing time, where the errors are the largest. Even then, the deviation from Gaussian distribution rises only for the extreme errors. This indicates that the linearization of the error minimization problem by eq 17 only negligibly distorts the normal distributions. Hence, the  $L$  values and  $\Delta L$  values obtained by eqs 30 and 31, for all practical purposes, may be considered as the maximum-likelihood values.

Although eqs 30 and 31 can be derived as the statistical averages of a number of measurements of parameter  $L_{ii}^k$  with errors  $\epsilon_{ij}^k \Delta a$ , we prefer to consider them as the least-squares error fit of eq 2 linearized by eq 17. Because eq 17 represents FMA, the whole least-squares procedure can be considered as a least error matrix analysis. Then it can be conveniently related to BU and FMA analysis as is schematically indicated in Figure 3. LEMA is a generalization of BU and FMA since, like BU, it takes into account the mixing time evolution of peak volumes and, like FMA, it keeps track of peak volume interdependence.

The LEMA error limits are smaller than the limits in either BU or FMA because LEMA combines all the available information in a least-squares manner. This is confirmed in a series of simulations presented in Table 1 where the LEMA errors are approximately half the errors of either BU or FMA. Even such a modest improvement in accuracy may be very important in the determination of low magnetization exchange rate constants.<sup>10</sup> For example, for Pro H $^{\alpha}$ -Gly H $^N$  in BU and FMA, the relative errors are larger than 100% and  $L$  cannot be determined. However, in LEMA the error is about 50% and  $L$  is determined as  $0.08 \pm 0.04 \text{ s}^{-1}$ .

The relationship between the LEMA and the FMA errors can be grasped from Figure 5b. Whereas the FMA error depends on the mixing time, the LEMA error is constant. As a compound error of all FMA errors (eq 31), the LEMA error is always smaller than the smallest FMA error. Figure 5b also shows the importance of performing experiments at different mixing times. Because LEMA attributes the highest weight to the  $L$  values with minimal error (eq 31), the LEMA error for each  $L_{ij}$  is always smaller than the minimal FMA error under given experimental conditions. In other words, LEMA guarantees that with a uniform spread of mixing times each  $L_{ij}$  has an error smaller than the minimal possible error of a single FMA at the optimal mixing time.

We believe that the reduction of error limits offered by LEMA increases the applicability of 2D exchange spectroscopy, enabling a reliable quantitative interpretation of the spectra.

## APPENDIX. EIGENSYSTEM OF QUASI-SYMMETRIC MATRICES

Let  $\mathbf{L}$  be a quasi-symmetric matrix, i.e.

$$\mathbf{L}\mathbf{N} = \mathbf{N}\mathbf{L}^T \quad (\text{A-1})$$

where  $\mathbf{N}$  is a positive (or negative) definitive diagonal matrix.

Let  $v_i$  and  $v_j$  be the left eigenvectors of  $\mathbf{L}$ , such that

$$\begin{aligned} \mathbf{L}^T v_i &= \lambda_i v_i \\ \mathbf{L}^T v_j &= \lambda_j v_j \end{aligned} \quad (\text{A-2})$$

Then

$$\begin{aligned} \langle \mathbf{L}^T v_i, v_j \rangle_{\mathbf{N}} &= \lambda_i \langle v_i, v_j \rangle_{\mathbf{N}} \\ \langle v_i, \mathbf{L}^T v_j \rangle_{\mathbf{N}} &= \bar{\lambda}_j \langle v_i, v_j \rangle_{\mathbf{N}} \end{aligned} \quad (\text{A-3})$$

where

$$\langle \mathbf{x}, \mathbf{y} \rangle_{\mathbf{N}} = \mathbf{x}^T \mathbf{N} \mathbf{y} \quad (\text{A-4})$$

defines an inner product. From eqs A-3, by subtraction

$$(\lambda_i - \bar{\lambda}_j) \langle v_i, v_j \rangle_{\mathbf{N}} = 0 \quad (\text{A-5})$$

If  $i = j$ , from eq A-5 it follows that

$$\lambda_i = \bar{\lambda}_i \quad (\text{A-6})$$

or  $\lambda_i$  is real.

From eq A-5 one can see that the left eigenvectors corresponding to two different eigenvalues are  $\mathbf{N}$ -orthogonal, i.e.

$$\langle v_i, v_j \rangle_{\mathbf{N}} = 0 \quad \text{for } i \neq j \quad (\text{A-7})$$

If  $\lambda$  is an eigenvalue of multiplicity  $m$ , then there are  $m$  linearly independent eigenvectors with this eigenvalue (we always suppose that our matrices are semisimple). Using the Gram-Schmidt process, it is possible to determine a set of linearly independent vectors within given  $m$ -dimensional subspace that are  $\mathbf{N}$ -orthogonal and also span the same subspace.

It is easy to  $\mathbf{N}$ -normalize a set of  $\mathbf{N}$ -orthogonal eigenvectors. Hence, we can say that the left eigenvectors of a quasi-symmetric matrix  $\mathbf{L}$  are  $\mathbf{N}$ -orthonormal, i.e.

$$\langle v_i, v_j \rangle_{\mathbf{N}} = \delta_{ij} \quad (\text{A-8})$$

or

$$\mathbf{V}^T \mathbf{N} \mathbf{V} = \mathbf{I} \quad (\text{A-9})$$

From eq A-9, it follows that

$$(\mathbf{V}^T)^{-1} = \mathbf{N} \mathbf{V} = \mathbf{U} \quad (\text{A-10})$$

The columns of  $\mathbf{U}$  are the right eigenvectors, while the columns of  $\mathbf{V}$  are the left eigenvectors of the matrix  $\mathbf{L}$ . Equation A-9 shows that the left and right eigenvectors are biorthogonal.

The diagonalization transformation for quasi-symmetric matrix  $\mathbf{L}$  is

$$\mathbf{V}^T \mathbf{L} (\mathbf{V}^T)^{-1} = \mathbf{V}^T \mathbf{L} \mathbf{U} = \mathbf{V}^T \mathbf{L} \mathbf{N} \mathbf{V}^T = \Lambda \quad (\text{A-11})$$

where

$$\Lambda = \text{diag}\{\lambda_1, \lambda_2, \dots, \lambda_N\}$$

This case of diagonalization, eq A-11, is simpler than the general case, because it is easier to calculate  $(\mathbf{V}^T)^{-1}$ , particularly when  $\mathbf{N}$  is a diagonal matrix.

Using the left and right eigenvectors, the matrix  $\mathbf{L}$  can be expressed as

$$\mathbf{L} = \mathbf{U} \Lambda \mathbf{V}^T = \mathbf{N} \mathbf{V} \Lambda \mathbf{V}^T \quad (\text{A-12})$$

or

$$L_{ij} = \sum_k u_{ik} v_{kj}^T \lambda_k = \sum_k n_i v_{ik} v_{kj}^T \lambda_k \quad (\text{A-13})$$

#### REFERENCES AND NOTES

- Jeener, J.; Meier, B. H.; Bachmann, P.; Ernst, R. R. Investigation of Exchange Processes by Two-Dimensional NMR Spectroscopy. *J. Chem. Phys.* **1979**, *71*, 4546–4553.
- Ernst, R. R.; Bodenhausen, G.; Wokaun, A. In *Principles of Nuclear Magnetic Resonance in One and Two Dimensions*; Oxford University Press: New York, 1987; Chapter 2.4, p 62.
- Wüthrich, K. *NMR of Proteins and Nucleic Acids*; John Wiley & Sons: New York, 1986.
- James, T. L.; Suzuki, E.-I.; Pattabiraman, N.; Zon, G. 2D NOE Full Relaxation Matrix Analysis and Molecular Mechanics Calculations for Structure Determination in Solution: DNA Fragments. *Bull. Magn. Reson.* **1987**, *8*, 152–157.
- Boelens, R.; Koning, T. M. G.; Kaptein, R. Determination of Biomolecular Structures from Proton-Proton NOE's Using a Relaxation Matrix Approach. *J. Mol. Struct.* **1988**, *173*, 299–311.
- Post, C. B.; Meadows, R. P.; Gorenstein, D. G. On the Evaluation of Interproton Distances for Three-Dimensional Structure Determination by NMR Using a Relaxation Rate Matrix Analysis. *J. Am. Chem. Soc.* **1990**, *112*, 6796–6803.
- Perrin, C. L.; Dwyer, T. J. Application of Two-Dimensional NMR to Kinetics of Chemical Exchange. *Chem. Rev.* **1990**, *90*, 935–967.
- Willem, R. 2D NMR Applied to Dynamic Stereochemical Problems. *Prog. NMR Spectrosc.* **1987**, *20*, 1–94.
- Huang, Y.; Macura, S.; Ernst, R. R. Carbon-13 Exchange Maps for the Elucidation of Chemical Exchange Networks. *J. Am. Chem. Soc.* **1981**, *103*, 5327–5333.
- Zolnai, Z.; Juranić, N.; Macura, S. *J. Phys. Chem. A* **1997**, *101*, 3707–3710.
- Macura, S. Full-Matrix Analysis of the Error Propagation in Two-Dimensional Exchange Spectroscopy. *J. Magn. Reson.* **1995**, *112*, 152–159.
- Perrin, C. L.; Engler, R. E. Quantitative Assessment by 1D-EXSY NMR of Stereoelectronic Control in Acid-Catalyzed Exchange between Stereoisomeric 2-Methoxy-1,3-dioxanes and Methanol. *J. Am. Chem. Soc.* **1997**, *119*, 585–591.
- Starzak, M. *Mathematical Methods in Chemistry and Physics*; Plenum Press: New York and London, 1989.
- Macura, S.; Fejzo, J.; Westler, W. M.; Markley, J. L. Influence of Slow Internal Motion in Proteins on Cross-Relaxation Rates Determined by Two-Dimensional Exchange Spectroscopy. *Bull. Magn. Reson.* **1994**, *16*, 73–93.
- Macura, S.; Ernst, R. R. Elucidation of Cross-Relaxation in Liquids by Two-Dimensional NMR Spectroscopy. *Mol. Phys.* **1980**, *41*, 95–117.
- Kumar, A.; Wagner, G.; Ernst, R. R.; Wüthrich, K. Buildup Rates of the Nuclear Overhauser Effect Measured by Two-Dimensional Proton Magnetic Resonance Spectroscopy: Implications for Studies of Protein Conformation. *J. Am. Chem. Soc.* **1981**, *103*, 3654–3658.
- Hyberts, S. G.; Wagner, G. Taylor Transformation of 2D NMR  $\tau_m$  Series from Time Dimension to Polynomial Dimension. *J. Magn. Reson.* **1989**, *81*, 418–422.
- Majumdar, A.; Hosur, R. V. Distance Estimation from NOE Data in Macromolecular Systems: A Quadratic Approach. *Biochem. Biophys. Res. Commun.* **1989**, *159*, 886–892.
- Fejzo, J.; Zolnai, Z.; Macura, S.; Markley, J. L. Analysis of Laboratory-Frame and Rotating-Frame Cross-Relaxation Buildup Rates from Macromolecules. *J. Magn. Reson.* **1989**, *82*, 518–528.
- Fejzo, J.; Zolnai, Z.; Macura, S.; Markley, J. L. Quantitative Evaluation of Two-Dimensional Cross-Relaxation NMR Spectra of Proteins: Interproton Distances in Turkey Ovomucoid Third Domain. *J. Magn. Reson.* **1990**, *88*, 93–110.
- Macura, S.; Farmer II, B. T.; Brown, L. R. An Improved Method for the Determination of Cross-Relaxation Rates from NOE Data. *J. Magn. Reson.* **1986**, *70*, 493–499.
- Bremer, J.; Mendz, G. L.; Moore, W. J. Skewed Exchange Spectroscopy. Two-Dimensional Method for the Measurement of Cross Relaxation in Proton NMR Spectroscopy. *J. Am. Chem. Soc.* **1984**, *106*, 4691–4696.
- Borgias, B. A.; James, T. L. Two-Dimensional Nuclear Overhauser Effect: Complete Relaxation Matrix Analysis. *Methods Enzymol.* **1989**, *176*, 169–183.
- Boelens, R.; Koning, T. M. G.; Van der Marel, G. A.; Van Boom, J. H.; Kaptein, R. Interactive Procedure for Structure Determination From Proton-Proton NOEs Using a Full Relaxation Matrix Approach: Application to a DNA Octamer. *J. Magn. Reson.* **1989**, *82*, 290–308.
- Borgias, B. A.; James, T. L. Mardigras: A Procedure for Matrix Analysis of Relaxation for Discerning Geometry of an Aqueous Structure. *J. Magn. Reson.* **1990**, *87*, 475–487.
- Leefflang, B. R.; Kroon-Batenburg, M. J. CROSREL: Full Relaxation Matrix Analysis of NOESY and ROESY NMR Spectroscopy. *J. Biomol. NMR* **1992**, *2*, 495–518.
- Bevington, P. R.; Robinson, D. K. *Data Reduction and Error Analysis for the Physical Sciences*; McGraw-Hill, Inc.: New York, 1992.
- Di Cera, E. Use of Weighting Functions in Data Fitting. *Methods Enzymol.* **1992**, *210*, 68–87.
- Thompson, W. J. *Computing for Scientists and Engineers*; John Wiley and Sons, Inc.: New York, 1992.
- Perrin, C. L. Optimum Mixing Time for Chemical Kinetics by 2D NMR. *J. Magn. Reson.* **1989**, *82*, 619–621.
- Macura, S. Evaluation of Errors in 2D Exchange Spectroscopy. *J. Magn. Reson.* **1994**, *B104*, 168–171.
- Kalk, A.; Berendsen, H. J. C. Proton Magnetic Relaxation and Spin Diffusion in Proteins. *J. Magn. Reson.* **1976**, *24*, 343–366.
- Von Dreele, R. B. Crystal Structure of Cyclo-L-Prolyl-Glycyl. Refinement of High-Angle Diffraction Data. *Acta Crystallor.* **1975**, *B31*, 966–970.
- Shapiro, S. S. In *Handbook of Statistical Methods for Engineers and Scientists*; Wadsworth, H. M., Jr., Ed.; McGraw-Hill: New York, 1990.
- Zolnai, Zs.; Juranić, N.; Macura, S. Full Matrix Analysis of Cross-Relaxation Fails in Fractionally Deuterated Molecules. *J. Biomol. NMR* **1998**, *12*, 333–337.

CI990107+